



The submarine fault scarp of the 2011 Tohoku-oki Earthquake in the Japan Trench

Hayato Ueda¹, Hiroshi Kitazato², Alan Jamieson³ & Pressure Drop Ring of Fire Expedition 2022 Japan Cruise Leg2 science team*

Rupture of the plate boundary fault during the 2011 Tohoku-oki earthquake with moment magnitude 9.0 is thought to have propagated to the trench. Surface exposure of the fault has not yet been confirmed because of great depths that are challenging to access and study. Using a manned submersible in the Japan Trench, we explored and visually assessed the seafloor near the epicenter. On the eastern slope of a thrust ridge 59 m high, which appeared after the earthquake, we found a 26 m high subvertical cliff regarded as the fault scarp. Cross-section analysis suggests an 80–120 m slip on the fault when assumed to dip at 45–30°, to build up the observed relief. The estimated larger displacement in the trench than in more proximal parts can be attributed to local enhancement of the slip by extension of the wedge above a subducting graben on the Pacific plate.

¹Department of Geology, Faculty of Science, Niigata University, 8050 Ikarashi-nincho, Nishi-ku, Niigata 950-2181, Japan. ²Danish Center for Hadal Research satellite office / School of Marine Resources and Environment, Tokyo University of Marine Science and Technology, 1-205, 4-5-7 Konan, Minato-ku, Tokyo 108-8477, Japan. ³Minderoo-UWA Deep-Sea Research Centre, School of Biological Sciences and Oceans Institute, The University of Western Australia, M470, Perth, WA 6009, Australia. *A list of authors and their affiliations appears at the end of the paper. ✉email: ueta@geo.sc.niigata-u.ac.jp

Multi-beam echo sounding (MBES) and multi-channel seismic (MCS) surveys^{1,2}, undersea geodetic records³, and inverted coseismic slip models^{4–6} based on seismic waves, geodetic, and tsunami observations, all proposed that the fault rupture of the 2011 Tohoku-oki earthquake propagated to the trench with a coseismic slip as large as 50 m or more (Fig. 1). The estimated displacements near the trench considerably vary depending on models⁷. It was also found that the previously flat, sediment-filled trench bottom was partly uplifted during the earthquake, resulting in new thrust ridges as high as 50 m². Such a juvenile and large (for a single event) seafloor feature of evidently coseismic origin had however never been directly observed, because it is situated at a depth of ~7500 m, which is beyond the operational depth range of most scientific submersibles and remotely operated vehicles. Therefore, the detailed topography, geological structure, and accurate amount of coseismic displacement at the shallower tip of the rupture is left unconfirmed, despite having great importance in relevance in understanding the processes of the great tsunami disaster.

The Tohoku-oki earthquake occurred on March 11, 2011, due to a rupture along the interface between the subducting Pacific plate and the hanging-wall Okhotsk plate, on which the northeastern part of the Honshu Island of Japan is located. On-land GPS stations⁸ in northeastern Honshu and seafloor geodetic stations^{3,9,10} in the forearc coseismically moved eastward, with horizontal displacements progressively larger toward the east. On the lower trench slope, displacement as great as 65 m⁷ was estimated based on the difference in bathymetry before and just after the earthquake^{1,2}.

MBES and MCS surveys^{1,2} also revealed prominent local subsidence and uplift both as much as 50 m on the lower trench slope and the trench floor, respectively (Fig. 2). The uplifts (thrust ridges) appeared on the previously flat trench floor (Fig. 3). Eastern margin of each ridge is bounded by a corresponding thrust fault dipping to the west². The thrusting has been regarded as a result of the earthquake fault movement², or of the coseismic landslide together with the subsidence on the lower trench slope¹¹.

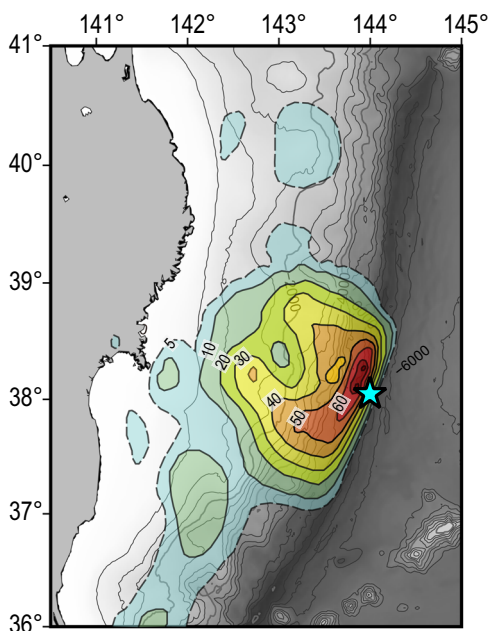


Fig. 1 Location of the study area. Topographic map is based on ETOPO1³². Blue star indicates the dive site. Colored contours show a coseismic slip model (in meter) based on geodetic data⁶.

According to drilling on the NW Pacific^{12–15}, the incoming oceanic sediments consist of Early Cretaceous chert (~70 m), unfossiliferous brown pelagic clay (~30 m), and Neogene to Quaternary siliceous mudstone (170–360 m), in stratigraphically ascending order. In MCS profiles^{2,16}, this oceanic sequence is tilted and dissected by normal faults of the horst-and-graben structure on the flexured Pacific plate (Fig. 2). A subducting graben is now present around the dive site at the Japan Trench axis. Horizontally settled trench sediments onlap the tilted oceanic sediments. JFAST C0019 drilling penetrated the frontal wedge overlying the subducting horst¹⁷. According to the drilling results, the wedge consists of tilted and faulted mudstone. The basal fault (décollement) beneath the wedge is identified as a shear zone <5 m thick¹⁸, and was formed at a horizon in the brown pelagic clay just above the chert section correlative to the incoming oceanic sequence^{19,20}. In the trench above the graben, the décollement transits into an upper stratigraphic horizon near the base of the trench sediments, from which imbricate thrust faults branch up to the flank of the thrust ridges^{2,16}.

In September 2022, the privately-owned full-ocean depth rated (11,000 m) submersible DSV Limiting Factor was used to dive to the bottom of the Japan Trench near the epicenter of the 2011 Tohoku-oki earthquake (Fig. 1). A high-definition video transect was made starting from the deepest part in the trench and ascended to the crest of a thrust ridge. Here, a large (26 m high) subvertical cliff was found and attributed to the surface expression of the 2011 earthquake fault tip. If the assignment is correct, it represents, to the best of our knowledge, the first direct observation and visual record of a fault scarp caused by a trench-type mega-earthquake that occurred along a subduction interface. Here we report on the dive results and discuss the events that occurred at the bottom of the Japan Trench and adjacent slopes during the earthquake.

Results

Topographic features around the dive site. The bathymetric map acquired in 2005²¹ (Fig. 3c) shows that the Japan Trench axis at 38°02' 05"N around the dive site was a flat basin floor without any obvious relief before the earthquake. The trench floor to the south of 38°03.5' (southern area) was 20–30 m shallower than that in the north (northern area), perhaps reflecting the basement structure. Longitudinal thrust ridges appeared within the trench floor in the 2011 map (Fig. 3b) acquired 11–12 days after the earthquake²², and the same features are still present in the 2022 map (Fig. 3a). The ridge in the northern area is convex westward and has asymmetric profiles with gentler slopes in the east and relatively steep slopes in the west. It is associated with lineaments corresponding to two west-dipping thrust faults (F3 and F4), and also potentially with an east-dipping back thrust (F2), referring to the MCS profile² (Fig. 2). Each of these lineaments shows a 20–30 m gap in elevation (Fig. 3b). In the southern area, the thrust ridge changes its shape to an arch convex eastward, with an asymmetric profile of the opposite polarity with steep slopes in the east and gentler ones in the west. Lineaments of the F3 and F4 faults in the northern area seem to merge to a single lineament (F4') bounding the eastern margin of the ridge in the southern area, with greater gaps of 40–50 m. The F2 lineament becomes indistinct toward the south. The difference in the ridge topography probably reflects the difference in fault geometry between the north and south areas. In the northern area, the total slip was probably distributed to two or three thrust faults (F2–F4) each having lesser displacement, whereas the slip seems to have concentrated to a single thrust fault (F4') with greater displacement in the southern area. Therefore, we expected that the thrust faults, if they really reached the surface, could more distinctly appear on the seafloor in the southern area than in the

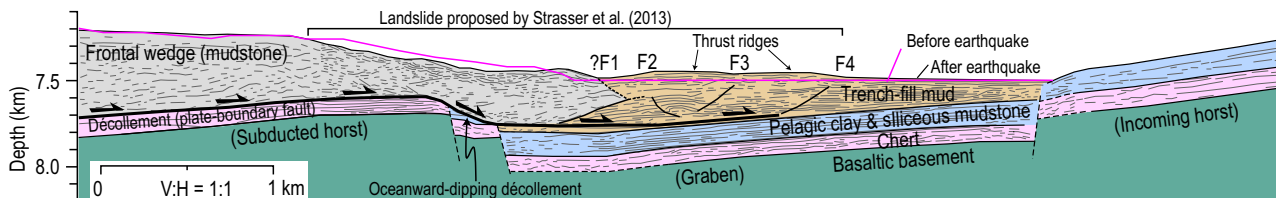


Fig. 2 Interpretative geological cross section near the dive site. Pre- and post-seismic topographic profiles and subsurface structures (seismic reflectors) are traced from MCS data². Geological assignments refer to the correlation between the drilling results of the frontal wedge and those of the Pacific Ocean floor²⁰. Labels ?F1 to F4 indicate faults in the trench axis. Geometries of F1 and F2 are our original interpretation, while those of F3 and F4 follow literature².

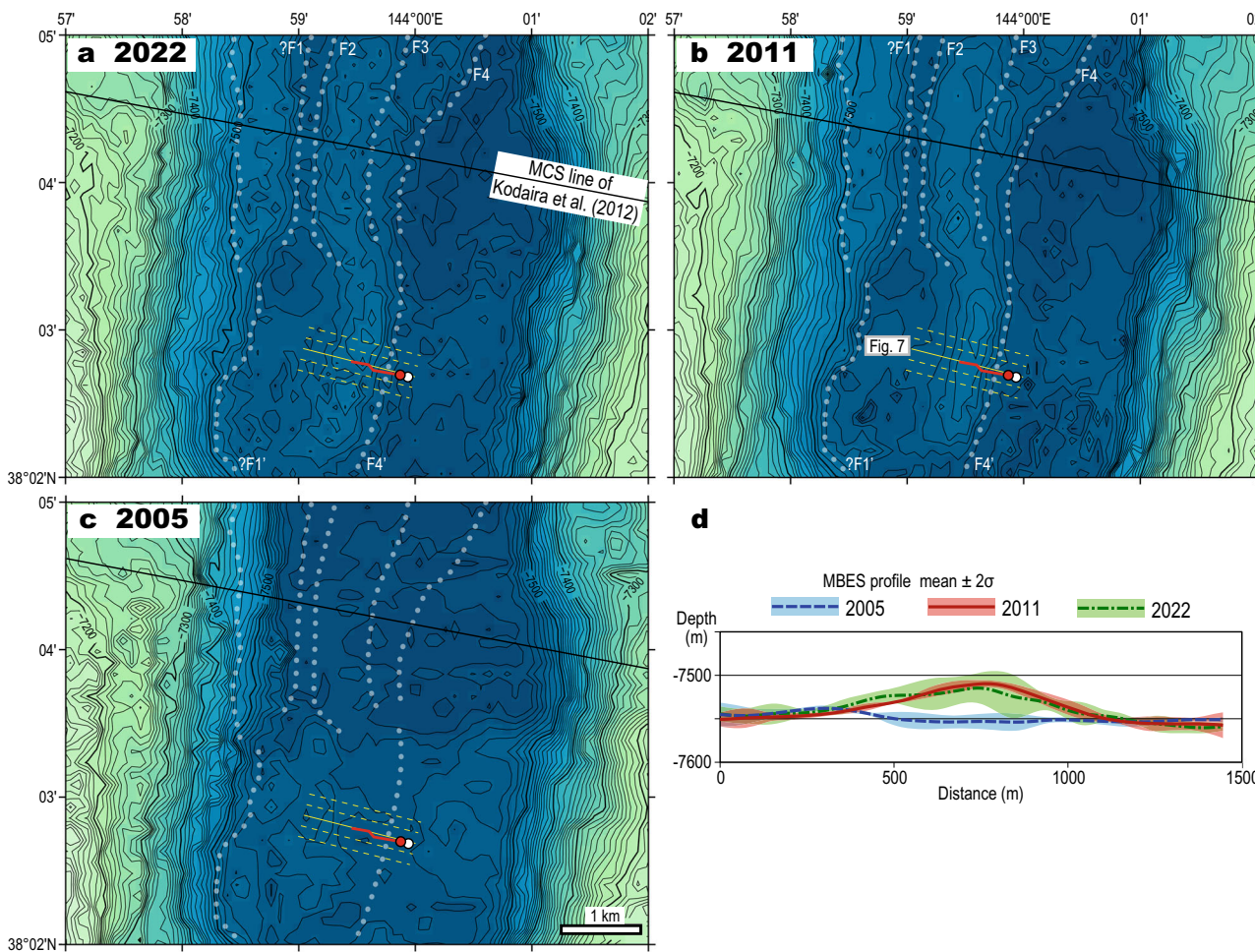


Fig. 3 Comparison of MBES bathymetry around the dive site before and after the 2011 Tohoku-oki earthquake. **a** The latest bathymetry map after the earthquake acquired on September 2, 2022, by the Pressure Drop Ring of Fire Expedition 2022 Japan Cruise Leg2. White dotted lines labeled as ?F1, F2, F3, and F4 show lineaments corresponding to thrust faults in the MCS profile² (Fig. 2), and ?F1' and F4' are presumable southern extensions of ?F1 and F4, respectively. White circles indicate the designated landing point, and red circles and lines indicate the inferable actual landing point of the lander SKAFF and the submersible DSV Limiting Factor, respectively. **b** Bathymetric map just 11–12 days after the earthquake on May 21–22, 2011, by JAMSTEC KR11-05 Cruise Leg2²². **c** The latest bathymetric map before the earthquake on July 2, 2005, by JAMSTEC KR05-07 Cruise²¹. Lineaments in the post-seismic maps are overlain for comparison. **d** Topographic cross sections of the 2005, 2011, and 2022 MBES data across the dive site. Each profile is represented by mean \pm double standard deviation (2σ) of the five parallel sections (yellow broken and solid lines in panels (a–c)) with a single-grid interval projected onto the central yellow solid line.

northern area, where traces of the faults could be indistinct or even blinded.

Dive results. We selected the dive site of the submersible Limiting Factor (dive #123) at a point in the southern area where the thrust ridge on the trench axis is singular and its relief is the most evident (Fig. 3). It lies ~ 2.5 km to the south of the MCS section line which depicted the thrust ridges², and ~ 12 km to the north of

the JFAST C0019 drill site¹⁷. The submersible landed on the seafloor to the east of the ridge flank at a depth of 7545 m as recorded by twin pressure sensors (see “Methods”). It traveled on a heading of 280° , except for the part heading 320° , where it had to face perpendicular to steep slopes (Fig. 4). The submersible transited up to the ridge crest with a depth of 7486 m, and left the bottom at 7490 m deep having completed a near 700 m horizontal transect (Supplementary Table 1).

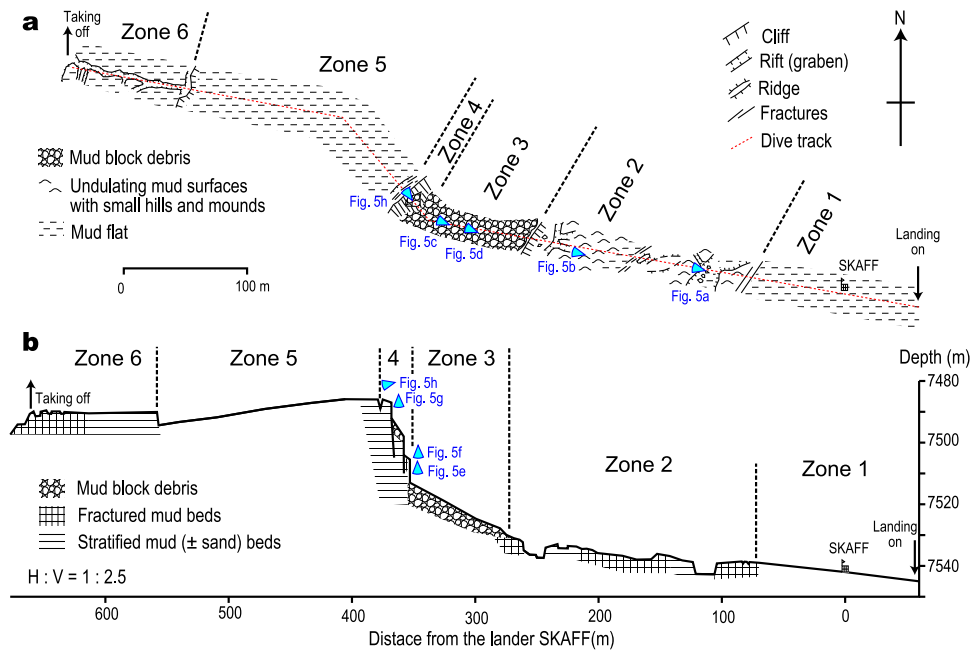


Fig. 4 Route map and cross section of the dive track of the submersible Limiting Factor dive #123. **a** Geological route map in horizontal view. **b** Topographic and geological cross section.

The dive track was divided into 6 zones on the basis of topographic features (Fig. 4 and Supplementary Table 2). Zone 1 was a mud flat very gently inclined to the east at $\sim 2^\circ$. Zone 2 was characterized by an undulating seafloor with many mounds of a few to several meters high (Fig. 5a), and partly with fissures and rifts several meters wide (Fig. 5b). Exposures on the rift wall suggested that the mounds consisted of somewhat damaged but still stratified mud beds (Fig. 5a). The average slope very gently inclined to the east at $\sim 3^\circ$. Zone 3 was a slope with increasing dip ($\sim 13^\circ$ on average) occupied by abundant angular blocks and clasts of somewhat compacted but soft mud (Fig. 5c). The mud blocks were characteristically polyhedral with sharp edges and planar to curvilinear surfaces (Fig. 5d), on which hackle marks were occasionally seen. Jigsaw cracks were common. All the blocks were covered by very recent mud no thicker than 1–2 cm (Fig. 5c, d). Zone 4 comprised subvertical cliffs (Figs. 5e–g and 6) totaling 26 m high and consisting of compacted soft mud beds, which were sub-horizontally stratified locally with thin sand layers (Fig. 6b). The cliff surfaces were planar to curvilinear with sharp edges (Fig. 6d). No trace of slip such as slickenside was seen, whereas hackle marks were common on the surfaces (Fig. 6d, e). Major fractures were subvertical and subparallel to the general cliff trend (Fig. 6c–e), and low-angle fractures were absent. Zone 5 above the cliff, comprising the ridge crest, was a smooth mud flat (Fig. 5h) gently inclined to the west at $\sim 2^\circ$. Zone 6 was marked by rifts several meters wide among mud flats. The submersible left the bottom at the head of a west-dipping slope or cliff.

Discussion

Significance of topographic features. Comparison of bathymetry before and after the earthquake (Fig. 3) shows that the thrust ridges were formed between 2005 and 2011, no later than 11 days after the earthquake. Because no large earthquake other than the 2011 event occurred in this area during the period, it is reasonable to attribute the uplifting of the thrust ridge on the dive site to the coseismic movement in 2011. As seen in the 2005 map (Fig. 3c), the seafloor of zones 5 and 6 was originally situated on the deepest level of the trench floor, and was elevated as high as 59 m

due probably to the earthquake. The zone 4 cliff marks the eastern edge (lineament F4' in Fig. 3) of the ridge as a continuation from the ridges with thrust faults (F3 and F4) in the MCS section (Fig. 2). Therefore, the zone 4 cliff is regarded as a surface expression of the F4' thrust fault, which lifted the seafloor of zones 5 and 6. However, no low-angle fault was observed, only subvertical fractures, and no slickensides but hackle marks are present on the cliff. Hackle marks are traces of propagating tensile fracture without slip²³. Therefore, the cliff surfaces are not the fault plane, but joint surfaces probably formed by the collapse of the elevated beds. Rock fall or topple rather than slides are compatible with the absence of any trace of slip on the surface.

The mud block debris observed in zone 3 was probably supplied from the zone 4 cliff. Highly angular block shapes (Fig. 5d) of the soft mud suggest that the blocks scarcely collided with or grinded against each other, and the abundant jigsaw fractures indicate fragmentation in situ with minimal subsequent rotation and transportation. These features support the idea that the mud block debris is the result of rock fall or topple rather than debris flow or a landslide. Because all the blocks are blanketed by thin mud, the fragmentation occurred very recently but is probably not currently active. Sedimentation rates near the dive site have been estimated as ~ 1 mm/year based on piston core analysis²⁴. Therefore, 1–2 cm thick uncompacted mud covers are not inconsistent with the interpretation that most of the debris was provided during the earthquake in 2011.

The undulating gentle slopes of zone 2 were also probably affected by the earthquake. The mounds consist not of debris but of somewhat damaged mud beds (Fig. 5a) and are thus considered as a feature of deformed beds such as small-scale folding. The deformation in zone 2 seems pervasive without any localization, in marked contrast to zones 4 to 6, where non-deformed sediments were uplifted by a deformation presumably localized to the underlying thrust fault. Contraction of the trench sediments in front (on the east) of the thrust fault (Fig. 7) could be responsible for the deformation. The undulation seems to have overprinted fissures (Fig. 5b) and was not observed on the elevated trench sediments of zones 5 and 6. These occurrences imply that the feature in zone 2 was formed by a slow and plastic

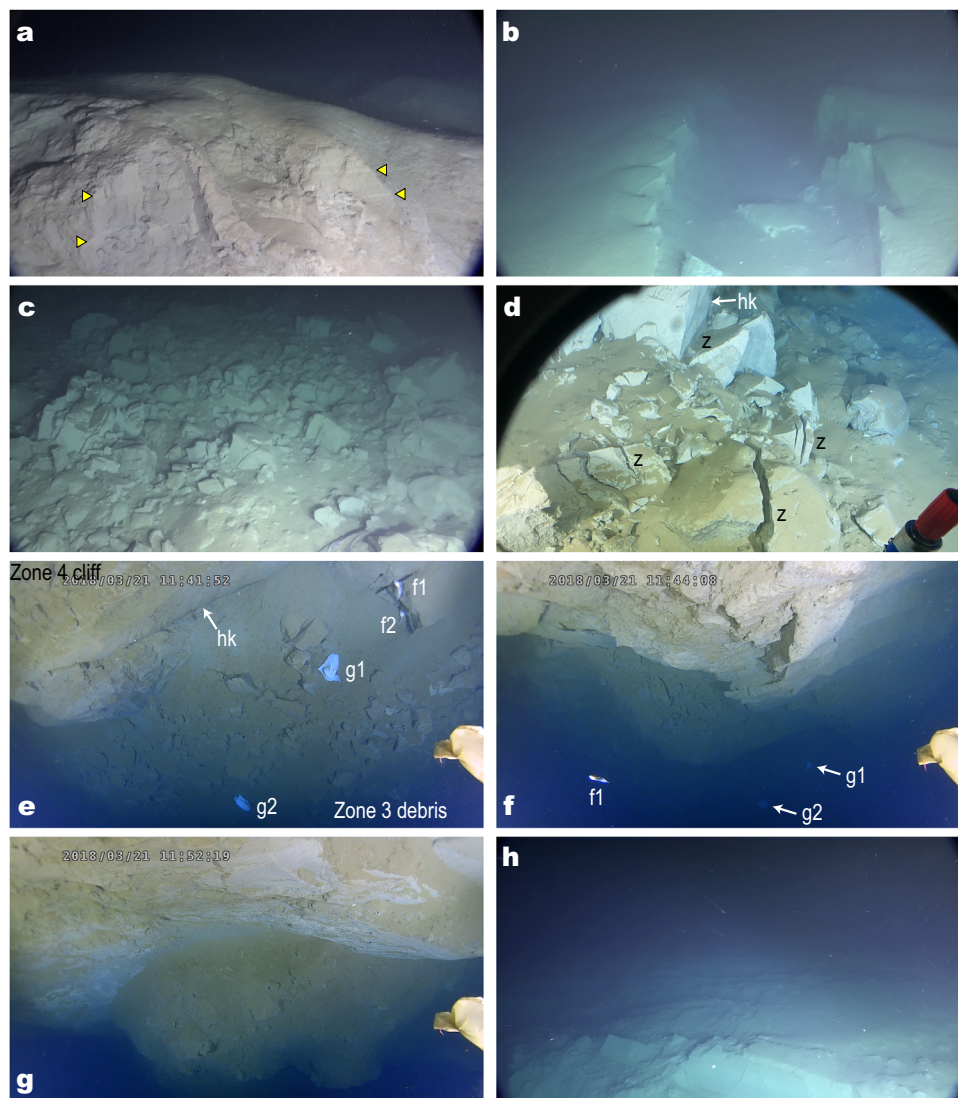


Fig. 5 Photographs of representative seafloor features observed during the submersible Limiting Factor dive #123. **a** An undulating seafloor in zone 2. Horizontal stratification (yellow arrows) of damaged mud exposed in front suggests that the mounds consist of deformed beds rather than debris. **b** A fissure ca. 2 m wide among undulating sea floors of cohesive mud beds in zone 2. Note that undulations on both sides do not match, suggesting that they postdated the fissure. **c** A typical slope in zone 3 consisting of mud block debris. **d** Angular mud blocks with jigsaw fractures (labeled as z) and hackle marks (hk). Note that beige white mud blocks are blanketed by darker-colored very recent mud. **e** Looking down the boundary between mud block debris in Zone 3 and a basal part of subvertical cliff in zone 4. Larger garbage plastic bag (labeled as g1) and a fish (f1) are approximated as 40 cm and 20–30 cm long, respectively. **f** Downward view of the middle parts of the cliff in zone 4. The same plastic bags (g1 and g2) as in photo **e** are still visible. The fish f1 chasing the ascending submersible is the same individual as that in photo (**e**). **g** Downward view from the top level of the cliff in zone 4. **h** Zone 5 flat seafloor just above the top of the zone 4 cliff. Rough surfaces with fractures in front grade into less deformed smoother mud flat beyond. Photos (**a–c**) and (**h**) are lateral views by forward camera. Photo (**d**) overlooks forward through a submersible window using a handy camera. Photos (**e–g**) are vertical views by downward camera (note that time stamps are erroneous).

deformation postdating the rapid upheaval of the thrust ridge. Slight tilting of the seafloor in zone 1 could also be faintly affected by the same contraction. Although little constraint is available for the origin of the deformation, here we suggest a possibility of sluggish uplift by plastic yielding of the soft mud bed to reduce the gradient of overburden owing to the rapid build-up of the thrust ridge (see also Supplementary Note 2 and Supplementary Fig. 3).

Thrust geometry and displacement. Based on the pressure sensor of the submersible, the difference in elevation between the basin floor and the thrust ridge crest was measured as 59 m with a

presumable error of ca. ± 1 m owing to uncertainty in the altitude of the vehicle (see the method). According to MBES acquired in 2011 and 2022, the gap was measured as 47 ± 6 m and 45 ± 8 m, respectively, which were significantly lower than the measurement by the submersible pressure sensor. The difference probably owes to the limited spatial resolution (no smaller than 130 m) of MBES at great depths, which could average the depths of the highest and surrounding lower parts. Considering the flat ridge crest observed during the dive (Fig. 4) and the small along-strike variation in MBES profiles (Fig. 3d), the 59 ± 1 m gap measured by the submersible can so far be regarded as a representative of the actual vertical displacement of the thrust fault around the dive site.

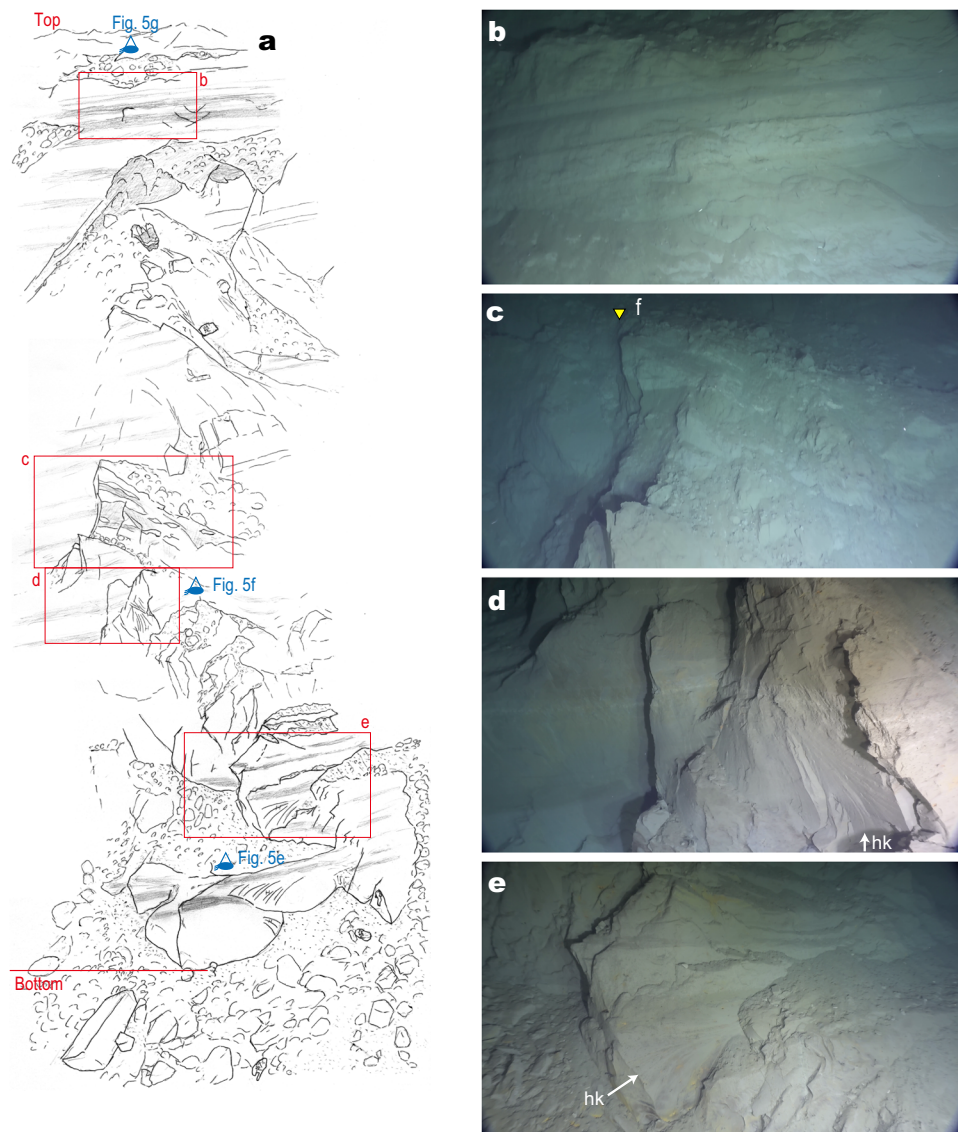


Fig. 6 **A sketch and snapshots of the cliff in zone 4 regarded as the 2011 Tohoku-oki earthquake fault scarp.** **a** A sketch of the whole section of the cliff (facing northwest), integrating features from video images of limited views. Scales are not accurate. The total height of the bedrock exposure (from the labels of bottom to top in the picture) is estimated as 26 m. **b** Undeformed, horizontally stratified mud beds intercalating thin sand layers at the top section of the cliff. **c** Deformed and tilted mud beds (center to right) abutting onto non-deformed mud beds (left) bounded by a minor secondary fault (yellow arrow labeled as *f*). **d** Stratified mud beds with subvertical to partly overhanging joint surfaces, on which hackle marks (*hk*) are visible. **e** Flaky appearance of the mud bed surfaces with dominantly northeast-trending parallel joints, on which hackle marks are seen.

No reliable constraint is available for the dip angle of the thrust fault ($F4'$) at the dive site. One of the simplest assumptions regards that the $F4'$ fault dips at $\sim 30^\circ$ as the $F4$ fault in the MCS profile does (Fig. 2). Because the dip angle of a fault beneath an initially flat surface (i.e., under purely horizontal compressive stress) is a function of frictional strength of the sediments, which may not greatly differ within a single basin (for detail, see Supplementary Note 2). Larger dip angles cannot still be rejected. However, they are considered as less plausible, because a steeper thrust fault forms in weaker sediments, and a 45° -dipping thrust fault requires zero friction.

Figure 7 shows a balanced cross section applied to the topography based both on MBES and submersible dive log, with an assumed thrust dip of 30° . A somewhat listric thrust fault fits better to the asymmetric profile of the ridge. The depth to the décollement, as a function of the thrust fault dip angle θ and the width of the ridge (see Supplementary Note 2), is estimated as

~ 230 m at $\theta = 30^\circ$ compatible with that determined by the MCS profile² but could also be as deep as 320 m when steeper θ up to 45° is assumed. Folding at the thrust front (fault-bend fold²⁵) is a common feature of thrust belts, but was not present here because all the exposed beds were scarcely tilted (Fig. 6b). Instead, abundant mud block debris occurs around the fault tip. The beds elevated by the fault were thus not folded but collapsed. Folding in soft sediments requires internal flow. Therefore, the absence of folding, coupled with brittle fracturing and fragmentation, implies that the stress increased so quickly that there was no time for viscous flow to release it. It supports the coseismic fast movement of the thrust fault. The mud block debris, whose volume should be balanced with that of the collapsed part, inferably comprises a small prism overridden by the thrust sheet (Fig. 7).

With an assumed dip angle of 30° , the 59 ± 1 m uplift of the thrust ridge is achieved by 118 ± 2 m slip along the fault. When a larger dip up to 45° is assumed, the slip necessary for the gap

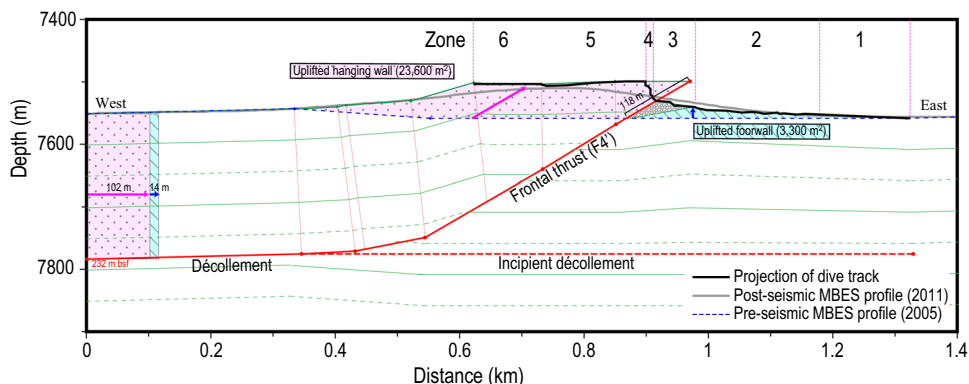


Fig. 7 A balanced cross section along the dive track adjusted to the observed topography. Location of the section line is shown in Fig. 3b. The section with an assumption of the thrust fault dipping at 30° is selectively shown. Sections assuming other dip angles of the thrust fault are shown in Supplementary Fig. 2. Pink and blue areas at the center show uplifted sections in the hanging wall and footwall, respectively. Those at the western end represent horizontal displacement to compensate for the corresponding uplifted masses.

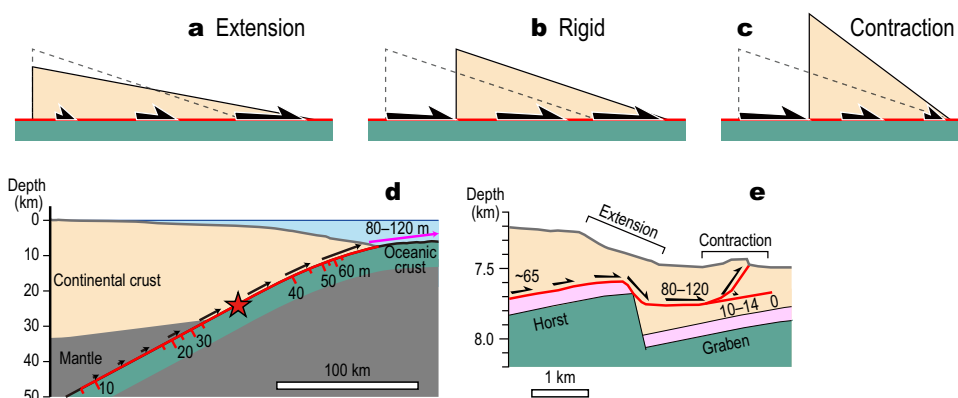


Fig. 8 Interpretation for heterogeneous coseismic slips. a–c Schematic relationship between the distribution of the basal slip and deformation in the sliding wedge. **a** The basal slip is progressively enhanced toward the toe of an extending wedge. **b** Homogeneous basal slip is expected beneath a parallelly sliding rigid wedge. **c** The slip is absorbed by the contraction of a wedge. **d** Geodesy-based coseismic slip model⁶ (red ticks and black arrows) and our estimate of the slip in the trench (magenta arrow) projected onto a section crossing the dive site. Slip distribution becoming larger toward the trench suggest bulk extension of forearc in the upper plate. **e** Close-up view of the trench axis. Numbers indicate the estimated coseismic slip in meters. Our estimation of the slip within the subducting graben greater than that above the horst⁷ suggests a local extension of the wedge above the oceanward-dipping graben wall. The sudden drop of the slip across the thrust ridge is a result of contraction concentrated to the wedge tip.

could be reduced to 83 ± 1 m. The amount of slip can also be estimated from mass balance of the uplifted volume with the depth to the décollement (Fig. 7 and Supplementary Fig. 2). With an assumption of 30°-dipping thrust fault, the uplifted mass is measured as $26,900 \pm 500 \text{ m}^2$ ($23,600 \text{ m}^2$ for the hanging wall, and 3300 m^2 for the footwall; see Supplementary Table 3) can be achieved by 116 ± 6 m slip on the décollement at the graphically estimated level of 232 ± 10 m below seafloor. Assuming a 45°-dipping thrust fault, the amount of slip is estimated as 79 ± 4 m. These mass balance-based slip values are in good accordance with the values based on the topographic gap. Therefore, the amount of coseismic slip at the trench axis can so far be estimated as large as 80–120 m, although the values should be tested by acquiring data of on-site sub-bottom structures and more detailed topography in the future.

The cause of the large slip. Our in situ observations support the idea that the fault rupture propagated to the surface in the trench^{1–6}. However, our estimation of the displacement as large as 80–120 m in the trench is greater than most of the previous estimates of coseismic slip in more proximal parts⁷. Overall, coseismic surface movements^{1–3,8–10} and the deduced slips on the plate interface^{4–6} were progressively larger toward the trench

(Fig. 8d). This trend suggests that the bulk forearc of the upper plate was laterally extended (Fig. 8a–c) during the earthquake, as the work of long-term subduction traction stored as gravity potential of the thickened wedge was released. This rebound could be analogous to an expanding spring releasing its internal elastic energy. Further large slip in the trench, as we estimated, is thus consistent with this general trend. The gradient of increasing slip, however, is quite large near the trench compared to more proximal parts of the wedge: ca. 65 m slip⁷ at the foot of the lower trench slope was increased to 80–120 m in the trench within several kilometers (Fig. 8e). Therefore, it is better to consider that the coseismic slip was locally enhanced near the trench axis. The lateral extension of the wedge toe, represented by subsidence on the lower trench slope (Fig. 2), probably led to local enhancement of the basal slip. This slope deformation, which has been formerly regarded as a landslide^{1,11}, occurred above the subducted graben margin, where the advancing wedge materials overpass the oceanward-dipping décollement. Here, the wedge materials are rotated forward, and over-steepened their surface slopes causing extensional failure^{26,27} (Fig. 8e, also see Supplementary Note 3 and Supplementary Fig. 4). The slope failure itself could have acted like a landslide. However, the failure occurred not independently but linked with the coseismic slip of the wedge, being

destabilized by transported materials into the slope. Therefore, it represents a locally extensional deformation in the frontal part of the entire advancing wedge.

Another factor that could stretch the wedge is the reduction of the basal friction²⁸ from static to dynamic (Supplementary Table 4). In more proximal parts, the décollement is planar lying in the horizon of smectite-rich pelagic clay^{18,19} with very low coseismic friction²⁹. Coseismic strain localizes into this lubricant décollement, whereas the overlying wedge supported by its higher internal friction is resistant and may not deform (see Supplementary Note 3), even if the basal friction decreased. The oversteepened lower trench slope in mechanical failure can sensitively deform applying to the reduced basal friction.

Both the effects of uneven décollement and reduced friction selectively stretch the wedge toe parts, resulting in local enhancement of the coseismic slip in the trench. Even if the graben was not present and local extension did not occur, the sediments in the trench would have been pushed by the frontal wedge, which advanced as far as ~65 m near the trench⁷ (Fig. 8e). Therefore, an estimated two-thirds (~65 m) of the total slip in the trench (80–120 m) was likely inherited from coseismic slip at the base of the frontal wedge, and the remaining one-third resulted from local enhancement by extension above the subducting graben wall.

Conclusions

This study is summarized as follows:

- (1) The manned submersible dive was conducted in the Japan Trench axis near the epicenter of the 2011 Tohoku-oki earthquake. We observed and visually recorded a sub-vertical cliff 26 m high and abundant mud block debris in the lower slope on the eastern edge of a thrust ridge.
- (2) The thrust ridge on the dive site was not present before the 2011 earthquake. The observed features suggest a very recent but currently inactive episode with fast movement explaining the origin of the cliff and debris. These lines of evidence all support the idea that the cliff was formed by the coseismic thrust fault movement, which uplifted the trench floor.
- (3) We measured the height of the ridge in situ as 59 m by the pressure sensor of the submersible. Assuming various thrust fault dip angles from 45° to 30°, the coseismic slip ranging from 80 to 120 m in the trench is deduced for the measured gap. These values are compatible with the uplifted volume of the thrust ridge.
- (4) The coseismic slip near the trench was probably enhanced by local extension above a subducting graben, in addition to the general trend with a progressively larger slip toward the trench suggesting a bulk extension of the entire wedge.
- (5) Although it is still under debate whether the thrust movement in the trench was a direct continuation of the plate boundary rupture or not, our in situ observation verified that the coseismic slip reached the surface.

Methods

Submersible dive. Manned submersible dive (#123 on 4 Sep.) was undertaken using a two-person vehicle DSV Limiting Factor (Triton 36000/2) with the support vessel DSSV Pressure Drop during the Ring of Fire Expedition 2022 Japan Cruise Leg 2 (29 Aug. to 19 Sep. 2022). A bathymetric site survey was conducted using Kongsberg EM124 multi-beam echo sounder (Kongsberg Maritime, Norway; 1° × 2° beam angle) with depths consequently corrected by the CTD (conductivity, temperature,

and depth) data acquired during the submersible dive³⁰. A transponding underwater modem (GPM300 Acoustic Modem, L3 Oceania, Fremantle, Australia) equipped on a lander SKAFF deployed onto the designated dive point was used for relative positioning of the submersible. Time, heading, depth, and distance from the lander were manually logged at key points (Supplementary Table 1). Depth and temperature were recorded by twin CTD probes (SBE 49 FastCAT, SeaBird Electronics, Bellevue, WA). The depth was measured with a resolution of 0.14 m and an accuracy of ±7 m. Positions and depths in the other points were interpolated assuming constant velocities. Altitude (the distance between the vehicle and the sea bottom) was not logged, and the depths of the seafloor are represented by those of the vehicle itself. Downward camera images suggest that the actual seafloor was 0–5 m (1.5 m on average) deeper than the submersible (see Supplementary Note 1 and Supplementary Fig. 1). No difference in height of the thrust ridge, measured as the topographic gap between the lowest and the highest points, was found between the cases with and without correction of altitudes. The difference in height could contain ca. ±1 m error propagated from the uncertainty of altitudes of two points in addition to the resolution of the pressure sensor. Video data were acquired using one externally mounted High-Definition (HD) video camera (IP Multi SeaCam 3105; Deep Sea Power and Light, San Diego, CA) and one 4K camera (IP Optim SeaCam-IPOSC-2080; Deep Sea Power and Light, San Diego, CA), illuminated by ten 15,500 lumen LED lights (LED-1153-A3-SUS; Teledyne Bowtech, Aberdeen, UK).

Cross section analysis. In the cross section, topography after the earthquake is represented by a combination of projections from the submersible dive track and MBES data acquired in 2011. Depths obtained by the submersible pressure sensor were adjusted to the MBES profile to ensure that the depth of the deepest point on the basin floor was identical, in order to remove any inconsistencies in our data due to the differing methods of measurement. Because both the lander and the submersible seemed to have drifted during descent, their landing positions were also adjusted to the MBES topographic map, so as sum of squared differences between the MBES profile and the moving averages of the submersible profile to be minimized. Topographies before and just after the earthquake were represented by MBES data acquired in 2005 (KR05-07 cruise)²¹ and in 2011 (KR11-05 Leg2 cruise)²² using R/V Kairei of Japan Agency of Marine Science and Technology (JAMSTEC). They were collected by SEABEAM 2112 (2 × 2° beam angle) equipped with the research vessel R/V Kairei with correction by XBT (expendable bathythermograph) profiles. Bathymetric grid data were generated using the "nearneighbor" command of GMT 6.4³¹. A grid interval of 0.075 min (~140 m) and a search radius of 0.25 km were applied to all of the 2005, 2011, and 2022 MBES data.

The balanced cross section in Fig. 7 was drawn using the kink approximation²⁵. The position of the frontal thrust fault was constrained by balancing the volumes of the collapsed part and mud block debris. Displacements of the thrust sheet above the décollement and the frontal thrust faults were set constant. Inferred volumes of collapsed parts and mud block debris are also balanced. More detailed explanations are given in Supplementary Note 2.

Data availability

Data and model outputs are available in the figshare repository: <https://doi.org/10.6084/m9.figshare.24460756>.

Received: 4 April 2023; Accepted: 15 November 2023;

Published online: 26 December 2023

References

- Fujiwara, T. et al. The 2011 Tohoku-Oki Earthquake: displacement reaching the trench axis. *Science* **334**, 1240 (2011).
- Kodaira, S. et al. Coseismic fault rupture at the trench axis during the 2011 Tohoku-oki earthquake. *Nat. Geosci.* **5**, 646–650 (2012).
- Kido, M., Osada, Y., Fujimoto, H., Hino, R. & Ito, Y. Trench-normal variation in observed seafloor displacements associated with the 2011 Tohoku-Oki earthquake. *Geophys. Res. Lett.* **38**, L24303 (2011).
- Ide, S., Baltay, A. & Beroza, G. C. Shallow dynamic overshoot and energetic deep rupture in the 2011 Mw 9.0 Tohoku-oki earthquake. *Science* **332**, 1426–1429 (2011).
- Lay, T., Ammon, C. J., Kanamori, H., Xue, L. & Kim, M. J. Possible large near-trench slip during the 2011 Mw 9.0 off the Pacific coast of Tohoku Earthquake. *Earth Planets Space* **63**, 687–692 (2011).
- Iinuma, T. et al. Coseismic slip distribution of the 2011 off the Pacific Coast of Tohoku Earthquake (M9.0) refined by means of seafloor geodetic data. *J. Geophys. Res.* **117**, B07409 (2012).
- Sun, T., Wang, K., Fujiwara, T., Kodaira, S. & He, J. Large fault slip peaking at trench in the 2011 Tohoku-oki earthquake. *Nat. Commun.* **8**, 14044 (2017).
- Ozawa, S. et al. Coseismic and postseismic slip of the 2011 magnitude-9 Tohoku-Oki earthquake. *Nature* **475**, 373–376 (2011).
- Sato, M. et al. Displacement above the hypocenter of the 2011 Tohoku-Oki Earthquake. *Science* **332**, 1395 (2011).
- Ito, Y. et al. Frontal wedge deformation near the source region of the 2011 Tohoku-Oki earthquake. *Geophys. Res. Lett.* **38**, L00G05 (2011).
- Strasser, M. et al. R/V Sonne Cruise SO219A & JAMSTEC Cruise MR12-E01 scientists. A slump in the trench: tracking the impact of the 2011 Tohoku-Oki earthquake. *Geology* **41**, 935–938 (2013).
- Shipboard Scientific Party. Site 304: Japanese magnetic lineations. *Initial Reports of the Deep Sea Drilling Project* **32**, 45–73 (U.S. Govt. Printing Office, 1975).
- Shipboard Scientific Party, Site 436: Japan Trench outer rise, Leg 56. *Initial Reports of the Deep Sea Drilling Project* **56 & 57 Pt. 1**, 449–458 (U.S. Govt. Printing Office, 1980).
- Shipboard Scientific Party. Site 581. *Initial Reports of the Deep Sea Drilling Project* **86**, 241–266 (U.S. Govt. Printing Office, 1982).
- Shipboard Scientific Party. Site 1179. In *Proc. Ocean Drilling Program, Initial Reports* **191**, 1–159 (Ocean Drilling Program, 2001).
- Nakamura, Y., Kodaira, S., Miura, S., Regalla, C. & Takahashi, N. High-resolution seismic imaging in the Japan Trench axis area off Miyagi, northeastern Japan. *Geophys. Res. Lett.* **40**, 1713–1718 (2013).
- Chester, F. M., Mori, J. J., Toczko, S., Eguchi, N. & Expedition 343/343T Scientists. Japan Trench Fast Drilling Project (JFAST). *Integrated Ocean Drilling Program Preliminary Report 343/343T* <https://doi.org/10.2204/iodp.pr.343343T.2012> (2012).
- Chester, F. M. et al. Structure and composition of the plate-boundary slip zone for the 2011 Tohoku-Oki earthquake. *Science* **342**, 1208–1211 (2013).
- Kameda, J. et al. Pelagic smectite as an important factor in tsunamigenic slip along the Japan Trench. *Geology* **43**, 155–158 (2015).
- Moore, J. C., Plank, T. A., Chester, F. M., Polissar, P. J. & Savage, H. M. Sediment provenance and controls on slip propagation: lessons learned from the 2011 Tohoku and other great earthquakes of the subducting northwest Pacific plate. *Geosphere* **11**, 533–541 (2015).
- JAMSTEC (2012) KAIREI KR05-07 Cruise Data. JAMSTEC <https://doi.org/10.17596/0001037> (2012).
- JAMSTEC (2012) KAIREI KR11-05 Leg2 Cruise Data. JAMSTEC <https://doi.org/10.17596/0001148> (2012).
- Pollard, A. D. & Aydin, A. A. Progress in understanding jointing over the past century. *Geol. Soc. Am. Bull.* **100**, 1181–1204 (1988).
- Kanamatsu, T., Ikehara, K. & Hsiung, K.-H. Stratigraphy of deep-sea marine sediment using paleomagnetic secular variation: refined dating of turbidite relating to giant earthquake in Japan Trench. *Mar. Geol.* **443**, 106669 (2022).
- Suppe, J. Geometry and kinematics of fault-bend folding. *Am. J. Sci.* **283**, 684–721 (1983).
- Davis, D., Suppe, J. & Dahlen, F. A. Mechanics of fold-and-thrust belts and accretionary wedge. *J. Geophys. Res.* **88**, 1153–1172 (1983).
- Dahlen, F. A. Noncohesive critical Coulomb wedges: an exact solution. *J. Geophys. Res.* **89**, 10125–10133 (1984).
- Willett, S. D. Dynamic and kinematic growth and change of a Coulomb wedge. *Thrust Tectonics* (eds. McClay, K. R.) 19–31 (Chapman & Hall, 1992).
- Ujiie, K. et al. Low coseismic shear stress on the Tohoku-Oki megathrust determined from laboratory experiments. *Science* **342**, 1211–1214 (2013).
- Bongiovanni, C., Stewart, H. A. & Jamieson, A. J. High-resolution multibeam sonar bathymetry of the deepest place in each ocean. *Geosci. Data J.* **9**, 1–16 (2021).
- Wessel, P. et al. The Generic Mapping Tools version 6. *Geochem. Geophys. Geosyst.* **20**, 5556–5564 (2019).
- NOAA National Geophysical Data Center. ETOPO1 1 Arc-Minute Global Relief Model. NOAA National Centers for Environmental Information <https://www.ngdc.noaa.gov/mgg/global/relief/ETOPO1/data/> (2009).

Acknowledgements

Caladan Oceanic LLC and Inkfish LLC provided this precious chance and fully supported our research. Captain Alan Dankool, Expedition Leader Ian Strachan (EYOS Expeditions), and all the crew of DSSV *Pressure Drop* facilitated our activities. Successful dives would not have been achieved without an operation by the submarine team conducted by Tim MacDonald. Christopher May was the pilot, who led to, and first saw the fault cliff during dive#123. The first author also thanks Kenichiro Tani for yielding his opportunity for embarkation. Suggestions by Akito Ogawa greatly helped us to estimate the altitude of the vehicle from video images. JAMSTEC kindly provided MBES archive data for our request. This study was supported by the European Research Council (grant no.669947), the Danish National Research Foundation (grant DNR145), and JSPS KAKENHI (grant JP20H02013).

Author contributions

H.U. made observations and geological mapping as the dive scientist and wrote the draft of the manuscript. H.K. and A.J. designated and conducted the geological surveys and the entire research project of the cruise, respectively. All the members of the Pressure Drop Ring of Fire Expedition 2022 Japan Cruise Leg2 science team contributed to onboard research activities, discussions, and editing of the manuscript.

Competing interests

The authors declare no competing interests.

Additional information

Supplementary information The online version contains supplementary material available at <https://doi.org/10.1038/s43247-023-01118-4>.

Correspondence and requests for materials should be addressed to Hayato Ueda.

Peer review information *Communications Earth & Environment* thanks Tianhaozhe Sun, Takeshi Tsuji, Toshiya Fujiwara, and the other anonymous reviewer(s) for their contribution to the peer review of this work. Primary handling editors: Sylvain Barbot and Joe Aslin. A peer review file is available.

Reprints and permission information is available at <http://www.nature.com/reprints>


Publisher's note Springer Nature remains neutral with regard to jurisdictional claims in published maps and institutional affiliations.



Open Access This article is licensed under a Creative Commons Attribution 4.0 International License, which permits use, sharing, adaptation, distribution and reproduction in any medium or format, as long as you give appropriate credit to the original author(s) and the source, provide a link to the Creative Commons license, and indicate if changes were made. The images or other third party material in this article are included in the article's Creative Commons license, unless indicated otherwise in a credit line to the material. If material is not included in the article's Creative Commons license and your intended use is not permitted by statutory regulation or exceeds the permitted use, you will need to obtain permission directly from the copyright holder. To view a copy of this license, visit <http://creativecommons.org/licenses/by/4.0/>.

© The Author(s) 2023

Pressure Drop Ring of Fire Expedition 2022 Japan Cruise Leg2 science team

Todd Bond³, Sara Cardigos⁴, Masayoshi Funaki⁵, Alan Jamieson³, Hiroshi Kitazato², Paige J. Maroni³, Hiroyasu Nanbu⁶, Joanne M. O'Callaghan^{7,15,16}, Takuma Onishi⁸, Silje W. Pedersen^{9,10}, Jaya Roperez¹¹, Hiroumi Tsuruzono¹², Hayato Ueda¹² ¹², Hiromi K. Watanabe¹³ & Tetsuro Yasuda¹⁴

⁴Center for Coastal and Ocean Mapping, Joint Hydrographic Center, University of New Hampshire, Durham, NH, USA. ⁵Freelance TV director, Las Vegas, NV, USA. ⁶Neotech Inc., Tokyo, Japan. ⁷National Institute of Water and Atmospheric Research, Auckland, New Zealand. ⁸Nippon Marine Enterprises, Ltd, Yokosuka, Japan. ⁹Nordcee & HADAL, Department of Biology, University of Southern Denmark, Odense, Denmark. ¹⁰Department of Geosciences, UiT The Arctic University of Norway, Tromsø, Norway. ¹¹Inkfish LLC, Seattle, WA, USA. ¹²NHK Enterprises, Inc, Tokyo, Japan. ¹³X-star, Japan Agency for Marine Science and Technology, Yokosuka, Japan. ¹⁴Timeless Vision Pro Inc, Fujisawa, Japan. ¹⁵Present address: Oceanly Science Limited, Wellington, New Zealand. ¹⁶Present address: The University of Auckland, Auckland, New Zealand.